Bulletin of Earthquake Engineering (2025) 23:1407–1429
https://doi.org/10.1007/s10518-024-02094-6

ORIGINAL ARTICLE

Fling amplitude inventory of near-fault strong motion recordings in Turkiye

Emrecan Adanır[1] · **Gülüm Tanırcan**[1]

Received: 31 July 2024 / Accepted: 28 December 2024 / Published online: 7 February 2025
© The Author(s) 2025

Abstract

The fling step, a significant near-field effect, has an adverse impact on long-period engineering structures. Despite early recognition by pioneers, identifying and processing the ground motions containing the fling step remains challenging due to conventional data filtering methods that ignore low-frequency components. This study investigates the recovery of the fling step from near fault records and by modifying and/or adding processing steps to previous methods, proposes a robust processing scheme for strong ground motion recordings in capturing fling amplitude. The proposed scheme's capability is verified through GNSS-derived displacements from global and Turkiye earthquakes. Subsequently, the method is applied to strong motion recording in the Turkish dataset ($Mw \geq 6$ shallow crust earthquakes recorded at $R_{JB} \leq 50$ km), resulting in a comprehensive inventory of fling amplitudes across multiple motion components. This inventory serves both engineering and earth sciences research by facilitating the evaluation of existing predictive models. In addition, a Türkiye-specific performance evaluation of existing predictive models is conducted using the presented database. Lastly, a refined fling amplitude prediction model, based on conformity with the presented fling inventory, is proposed. This work addresses critical gaps in strong ground motion analyses, promoting improved seismic resilience through accurate characterization of near-fault effects.

Keywords Fling step · Near-fault · Permanent displacement · Seismic recording processing · Baseline correction · Strong ground database · Long-period motion

✉ Gülüm Tanırcan
birgore@bogazici.edu.tr

Emrecan Adanır
emrecanadanir@gmail.com

[1] Earthquake Engineering Department, Kandilli Observatory and Earthquake Research Institute, Bogazici University, Istanbul, Turkey

1 Introduction

Strong ground motions in the vicinity of a fault are generally dominated by earthquake source properties. One distinct characteristic of the near-fault strong ground motions (SGM) is the fling step. It is the permanent displacement (PD) observed at the displacement waveform of the SGM and manifests itself as a one-sided pulse on velocity time histories.

Experiences have shown that near-fault effects should be taken into account in the seismic design of particularly long-period structures. While pioneering studies on the fling effect show the existence of fling in SGM (e.g. Sasani and Bertero,2000, Erdik 2001; Alavi and Krawinkler 2001; Stewart et al.,2002, Abrahamson,2002, Rathje et al.2006), with the increase in recorded and simulated SGM recordings, in later studies the subject has been investigated in many aspects. (e.g. Kalkan and Kunnath 2006; Ucak et al., 2014, Yang et al. 2010; Hamidi et al. 2018; Jamnani et al. 2013; Yadav and Gupta,2017, Bhagat et al.,2018, Gholipour et al. 2023).

For seismic design of structures under near field ground motion excitation, codes such as International Building Code (IBC, ICBO 2006) and California Building Code (CBC, ICBO 2007), which are based on ASCE7-22 (ASCE 2005), recommend selecting strong motion recordings including pulse characteristics of the motions for use in nonlinear response history analysis of structures. Nonetheless, ground motion recordings containing the fling step cannot be identified since common data processing schemes, like filtering, ignore the low-frequency parts of the strong motions and thus mask the fling effects.

There are three main approaches to obtaining the fling containing ground motion recordings. The first approach is based on obtaining artificial recordings by using different simulation techniques (Hisada and Bielak 2003; Hamidi et al. 2018; Wu et al. 2020; Hisada and Tanaka 2021). Nevertheless, using synthetic recordings in non-linear time history analyses results in lower demand than actual ones (Hamidi et al. 2018). The second approach is to produce the artificial fling step by theoretical approach and then superimpose on the real filtered motions (e.g. Abrahamson 2002; Kamai et al. 2014). This approach gives rise to a conservative estimate of the collapse capacity and is found to be questionable (Burks and Baker,2014). The last approach is processing the real recordings by special data processing schemes (e.g. Iwan et al. 1985; Boore 2001; Wu and Wu 2007; Chao et al. 2010; D'Amico et al., 2018, Schiappapietra et al. 2021). Regarding the third group, all the existing data processing schemes rely on baseline correction of the separate parts of the recordings. As a pioneering research, Iwan et al. (1985) proposed a new baseline correction algorithm consisting of the evaluation of the baseline shifts in the strongest part of the motion and the last part, that are separated by time correction points. After the 1999 Chi-Chi earthquake (Mw7.6), Boore (2001) inspected the scheme and redefined the correction points of the previous algorithm. The improvements continued by Wu and Wu (2007), who altered the methodology by dividing the ground motions into 3 windows as well as linking the detection of the corrected trace to the flatness of the last portion. Following them, Chao et al. (2010) clarified the selection of the correction points by associating them with cumulative dissipated energy. Recently, a semi-automatic data processing scheme, extended Baseline Correction procedure (eBASCO), has been introduced by D'Amico et al. (2018) and upgraded by Schiappapietra et al. (2021). Although the eBASCO has various advantages compared to the previous schemes, applications of the eBASCO with new SGM recordings have shown that the method has aspects that could be improved. For instance, with the improvements,

the scheme can be exposed to much more diverse ground motion records. In addition, the complexity of the eBASCO such as filtering and tapering steps could be clarified.

In this study, the eBASCO procedure of Schiappapietra et al. (2021) is enhanced by modifying and/or redefining certain steps to make the processing scheme more convenient and comprehensive. The proposed scheme is validated by comparing the permanent displacements in processed time histories from both Türkiye and worldwide earthquakes with those derived from co-located GNSS stations. Subsequently, the scheme is applied to the Turkish strong motion dataset, resulting in the Turkish fling amplitude inventory containing recordings in horizontal and vertical components (EW, NS, UD), fault normal (FN) fault parallel (FP), and maximum directions (RotD100), which is defined as the rotated motion yielding the maximum horizontal permanent displacement. The primary purpose of this dataset is to provide researchers with a detailed source of fling-containing recordings for use in engineering and earth science studies. Additionally, the presented inventory has been utilized to evaluate the performance of Kamai et al. (2014), Burks and Baker (2016) and Schiappapietra et al. (2022) fling step prediction models in Türkiye. Furthermore, a predictive model is proposed by adjusting Burks and Baker (2016) model to fit the presented dataset.

2 Methodology

Existing baseline correction algorithms to recover PDs date back to Iwan et al. (1985). They considered the baseline shift to be a result of hysteresis in the seismic transducers observed in the stronger parts of the recordings. They defined the stronger part of a motion between time correction points, namely T_1 and T_2, corresponding to the first and the last excursions of acceleration exceeding 50 cm/s2. Following the 1999 Chi-Chi earthquake (Mw7.6), Boore (1999, 2001) investigated recordings of the event and suggested that baseline shifts might also be due to ground tilting. Consequently, Boore (2001) redefined correction points, allowing T_1 to be a free parameter. However, this approach leads to intensive computational load mainly because of the nearly infinite possible combinations of time correction points, limiting its application to a small number of ground motion recordings (e.g. Kalkan and Kunnath 2006; Yadav and Gupta 2017). Wu and Wu (2007) altered the methodology by dividing the ground motions into three windows and linking the correction to the flatness of the last portion of the waveform. Their procedure was valid only for the recordings having a peak ground acceleration (PGA) of 60 cm/s^2 or higher. Chao et al. (2010) clarified the selection of the correction points by associating them with the first and last 50% of the cumulative dissipated energy, though computation load remained as issue due to numerous combinations of the possible time correction points.

D'Amico et al. (2018) proposed the eBASCO semi-automatic processing scheme, which did not contain any PGA limitation. This scheme relies on a baseline adjustment of the SGM recordings by means of a piecewise linear detrend, using trilinear rather than bilinear trending. The procedure includes the following steps: (1) subdividing the acceleration time history into pre-event, transient, and post-event windows by correction points T0, T1, T2, and T3. T0 correction point was defined as the first sample after subtracting the first sample of recorded motion to guarantee that the velocity starts from 0; T_1 is selected as one of the 5 points of correspondence which are logarithmically spaced from 0.0001 to 5% of the cumulative energy dissipation of the record; T3 is set to linearly spaced 5 samples between 50%

and % 95 of the cumulative energy dissipation of the motion; T_2 is sampled as 20 points that are logarithmically spaced from T_3 to the end of the record. (2) Applying detrending to each window. The baseline of the pre-event window is computed as:

$$V_i = A_i t \tag{1}$$

where t is the time and Ai is the slope of the line that fits the velocity trace in the pre-event window. Another least-squares fitting is used to remove the linear trend Vf in the post-event window of the velocity time history, which is defined as:

$$V_f(t) = V_{0,f} + A_f t \tag{2}$$

where Af is the slope of the line fitting the post-event window velocity and V0,f is the intercepting ordinate. In the scheme, the baseline correction Am, which was first defined as the intermediate range correction acceleration by Iwan et al. (1985), obtained as:

$$A_m = \frac{V_f(T_2)}{(T_2 - T_1)} \tag{3}$$

Am is used in the acceleration transient window to satisfy that the velocity at the end of the transient window oscillates around zero after the baseline correction. The velocity of the baseline correction at the end of the transient window should be equal to the velocity amplitude acquired from Eq. 2 as Vf (T2). (3) The corrected displacement and acceleration waveforms are obtained through integration and the derivation of the corrected velocity trace, respectively. (4) To avoid spurious spikes, the processed waveform is checked by following the condition that the acceleration amplitudes in T_1 and T_2 of the corrected waveform are conditioned to be less than 25% of the PGA. 5) The corrected waveform is pinpointed as the one that results in the maximum flatness among different trials, which are the combinations of different values for correction points, by using the "f-value" introduced by Wu and Wu (2007) after modifying it as:

$$f = \frac{r}{|b|\,\sigma} \tag{4}$$

where r is the linear correlation coefficient b is the slope of the least-squares regression line of the processed displacement trace from T_3 to the end of SGM, and σ is the variance the variance of the PD.

Schiappapietra et al. (2021) further enhanced the eBASCO procedure by incorporating a cosine taper at the beginning of the waveform and comparing acceleration amplitudes at the correction points before and after processing. The modified scheme involves: (1) cutting the uncorrected acceleration time history; (2) assigning the time correction points; (3) executing a tri-linear detrend on the velocity trace; (4) determining the best solution.

As the first step of the updated version of eBASCO, different from the previous one, a preliminary cutting of the acceleration time history is applied. Secondly, the first acceleration amplitude is subtracted from the acceleration time history to make the velocity zero at T_0. Just like the second step, time windows and the time correction points are defined in the

same way as the previous version of the eBASCO procedure. Moreover, the applied baseline corrections to pre-event and transient windows given by a linear trend between V_i (T_1) and V_f (T_2) were not changed in this scheme. However, to eliminate the unsuccessful combinations of the time correction points that result in spurious spikes on acceleration traces, Schiappapietra et al. (2021) proposed a different condition from the previous version of the scheme. For this purpose, they stated that the relative differences of the acceleration amplitudes in correction points T_1 and T_2 on the corrected and the raw data should be less than 25%. As the last step of the procedure, among all the combinations of the correction points, that meet the relative difference condition, the best solution is determined in the same way as the previous version of eBASCO. Nevertheless, while obtaining the final velocity and displacement traces, Schiappapietra et al. (2021) also recommend to use of cosine taper in each integration step as well as the second-order low-pass filter.

Both versions of the scheme rely on a baseline adjustment of the SGMs by applying a trilinear detrend. Nevertheless, there are still some deficiencies that need to be eliminated even after Schiappapietra et al. (2021). For instance, the initial signal cut at the beginning of the processing, cosine taper application, and low-pass filtering may vary for each recording; in other words, these steps lead to complexity and inconsistency. Additionally, both versions of eBASCO assign a very limited number of samples to the time correction points among their defined ranges and ignore most of the other possible samples, which paves the way for inaccuracy. Furthermore, assuming a linear detrending for each part of the record does not provide the time history similar to a ramp function shape. Moreover, the ambiguousness of the endpoint of the record causes different results, especially for the recordings with large PDs.

To address these issues, a new, comprehensive and feasible data processing methodology is proposed. The new procedure consists of mainly seven steps. (1) After reading the raw earthquake data, the first amplitude of the acceleration time history is assigned as zero to make sure that the velocity oscillates around zero at the beginning of the motion. (2) The SGM is divided into three time windows, namely pre-event, ephemeral, and post-event, by the time correction points T1, T2, and T3 and the possible samples for these points are assigned as the samples within defined ranges. Figure 1 demonstrates the example of assigned points on a corrected SGM.

(3) Least-linear fitting in pre-event (Eq. 1) and ephemeral (Eq. 3), and constant detrend in the post-event window are applied. Constant detrend is defined in Eq. 5, where j is the time, Tend is the end time of the record, T2 is the second correction point, and n is the number of the data in the post-event window of the recording. Vf is the baseline shift in the post-event window of the velocity time history, implemented at velocity time history as baseline corrections.

$$V_f = \frac{\sum_{j=T_2}^{T_{end}} V_{f,2}(j)}{n} \tag{5}$$

$$V_f = \frac{\sum_{j=T_2}^{T_{end}} V_{f,2}(j)}{n} \tag{6}$$

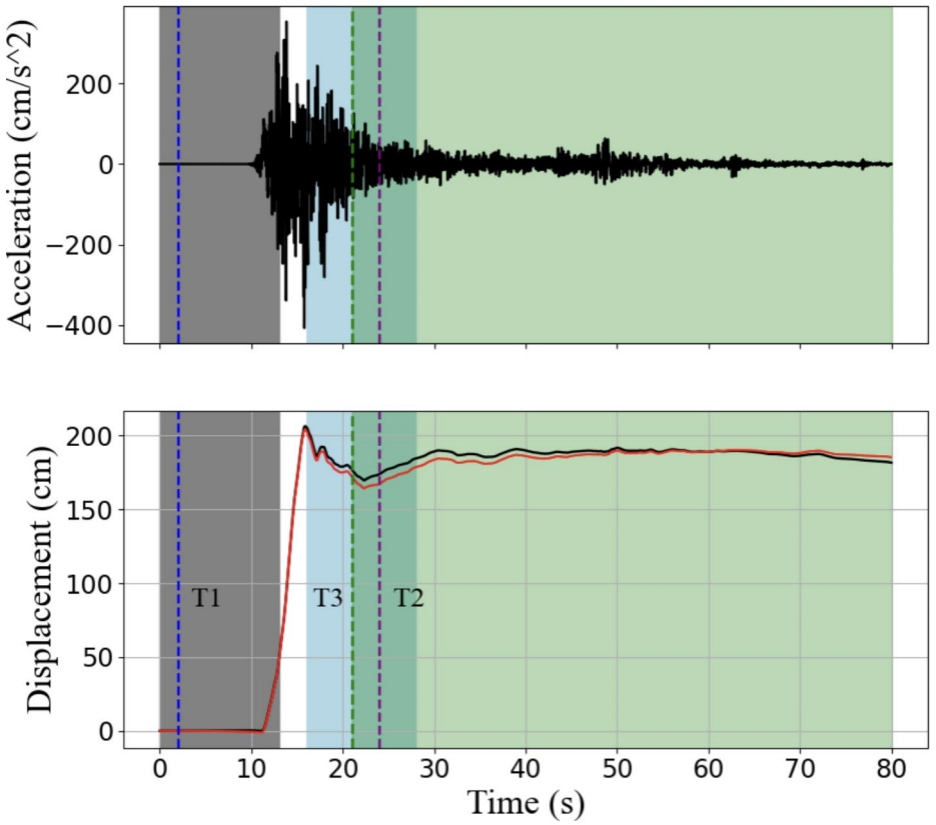


Fig. 1 The 1999 Kocaeli earthquake (Mw7.6) SKR station East-West component (above) acceleration and displacement (below) time histories with time correction points (dashed vertical lines) and the possible data ranges (shadowed)

(4) The three windows are concatenated to acquire the partly corrected velocity time history. Then, to check the conformity of the previous baseline corrections, another baseline is defined in the part of the motion from T3, where the strongest pulse of the motion finishes, to the end of the motion as Eq. 6., Vf,2 is the last baseline defined on the partly corrected velocity waveform between T3 and the end of the trace and other symbols are defined as Eq. 5. In addition, this step may be repeated arbitrarily as an additional correction, T(A), in the case of encountering a distinct, unexplained source of baseline shifts, which is out of the scope of this study.

(6) After differentiating the velocity trace into acceleration time history, there might be erroneous spurious spikes, only at the points that correspond to time correction points, emerge on the obtained acceleration time history. These spikes are detected after visual inspection of some of the records. Then, in the scheme, they are treated as one of the nonstandard errors that mask and distort the true record defined by Boore and Bommer (2005) and Puglia et al. (2018). Therefore, to make the acceleration trace of the correction motion appropriate to use in nonlinear time history analyses, Boore and Bommer

(2005)'s approach, removing the spikes and assigning the average of the samples before and after the spike sample, is recommended in this study. In addition, to avoid unphysical jumps that are not spurious spikes but rather a continuing distorted trace that stems from an inappropriate combination of the time correction points, the acceleration amplitudes of the raw and processed data corresponding to T1 are checked to make sure the difference is less than 25%. In this step, if the difference is found higher than 25%, then that combination of the time correction points is eliminated from the comparison of other combinations to decide the final solution. This step is not encountered within the extent of this study; nevertheless, it is introduced to the procedure based on D'Amico et al. (2018)'s findings. (6) The corrected waveform among overall combinations of the correction points is selected based on the fade level indication value (Eq. 4), whose maximum value demonstrates the minimum dispersion in the last portion of the motion from T3 to the end of the record. (7) As the last step, after obtaining the corrected waveform, the permanent displacement is assigned based on the Significant Duration theorem, presented by Trifunac and Brady (1975). It is assumed that after 95% of the cumulative energy of the strong ground motion is dissipated, the ground displacement fades by oscillating around the PD level. The flowchart of the proposed processing scheme is shown in Fig. 2.

Major improvements of the eBASCO scheme can be summarized as:
(1) Enhanced Time Correction: The time correction points are now assigned in seconds so that the number of the sample points taken into consideration is considerably increased, which is required for obtaining more accurate results;
(2) Constant Detrending: The execution of constant detrending in the post-event window portion together as well as the last detrend in the follow-up step of the procedure ensures the shape of a ramp function which was observed as the case for the displacement waveforms of fling-containing recordings (Boore 2001; Wu and Wu 2007). An example of displacement time history of a fling-containing SGM record, that has a ramp-like trace, and its time correction points are illustrated in Fig. 1.
(3) Removal of Spurious Spikes: Spurious spikes at the time correction points on the acceleration trace are removed by the acceleration amplitudes of the spikes with the mean of the data points on either side according to Boore and Bommer (2005);
(4) Fade Level Determination: Based on the Significant Duration theorem, (Trifunac and Brady 1975), it is assumed that after 95% of the cumulative energy is dissipated, the ground displacement fades by oscillating around the PD level, also defined as the fade level. Given that the NESS 2.0 database, which presents worldwide PDs using the eBASCO method by D'Amico et al. (2021), contains only a few recordings from Türkiye earthquakes, the feasibility of the proposed scheme is first evaluated using Türkiye SGM dataset. For this purpose, the SGM recordings with known PDs through site observations and derivations from co-located GNSS stations are processed by both eBASCO and the proposed scheme. An example of the comparison is exhibited in Fig. 3. Subsequently, the effectiveness of the proposed scheme in capturing PD is verified by comparing the derivations from GNSS data for both Türkiye and worldwide earthquakes, as presented in the next chapter of this study.

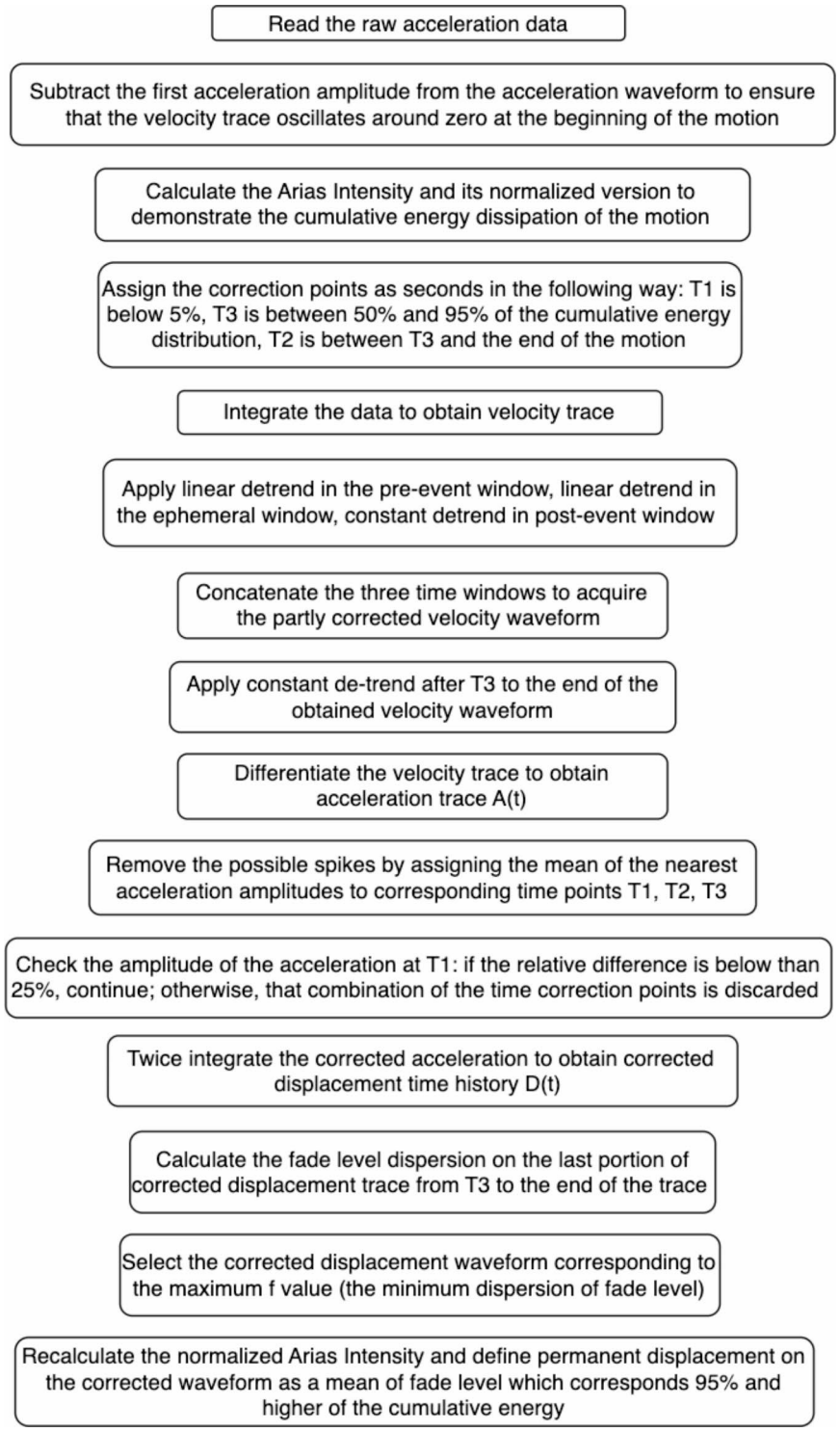


Fig. 2 The schematic illustration of the proposed data processing scheme

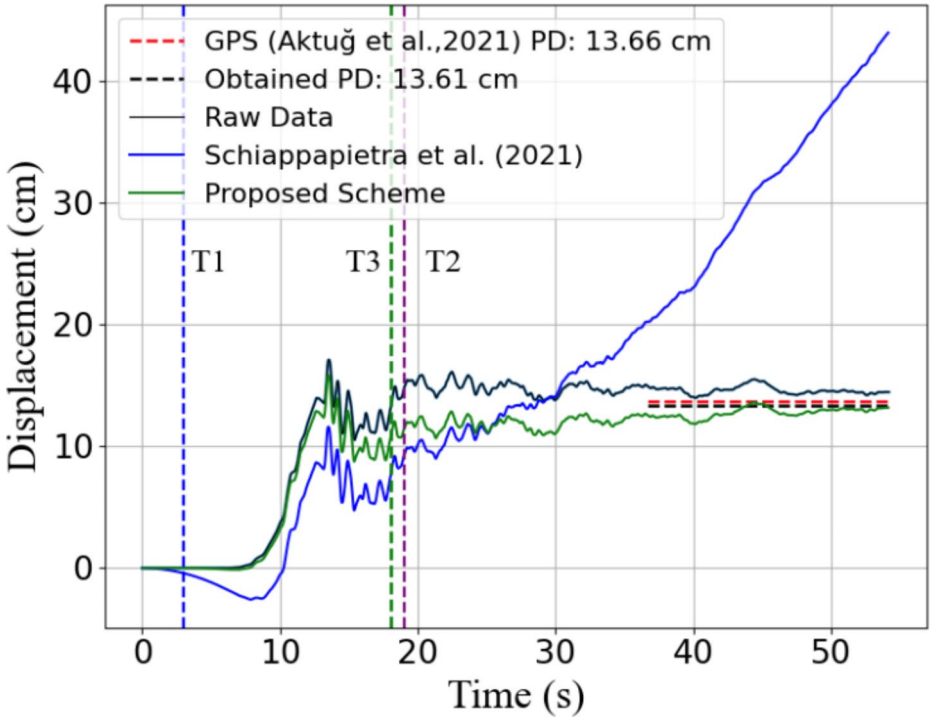


Fig. 3 Comparison of eBASCO (blue) and proposed processing scheme (green) with the time correction points and their ranges in the proposed scheme on the 2020 İzmir-Samos earthquake (Mw7) GMLD station North-South component displacement waveform. PD obtained with raw data the proposed scheme (and GNSS are shown with gray, dashed black and dashed red lines, respectively

2.1 Verification of the proposed scheme

For the verification of the proposed scheme, SGM recordings co-located with GNSS stations are collected from past worldwide earthquakes. A total of 25 recordings from 7 earthquakes with Mw between 6.5 and 7.6 and R_{JB} distance is up to 50 km are utilized. The comparison of the PDs calculated from SGM recordings and those derived from the GNSS stations are presented in Fig. 4; Table 1. To evaluate the proposed procedure from a wide perspective, records from the earthquakes including three styles of faulting are evaluated.

[a]: P43 indicates the location of the PD derived from satellite imagery. [b]: PD is given in absolute value.

As presented in Table 1, the GNSS-based PDs range from 0.25 cm to 260 cm, while procedure-based PDs on the co-located recordings range from 0.17 cm to 264.78 cm. Similarly, the distribution of the PDs from both sources aligns closely around the 1:1 line in Fig. 4, indicating the effectiveness of the proposed scheme in accurately revealing the PDs. In addition, it is proven that the procedure works for the records from all three kinds of styles of faulting earthquakes. To exemplify the effectiveness of the proposed scheme for both small and large PDs, Fig. 2 demonstrates the 1999 Chi-Chi (Mw.7.6) earthquake, reverse faulting earthquake, EW component of station TCU 137 and the 2014 Aegean Sea, strike

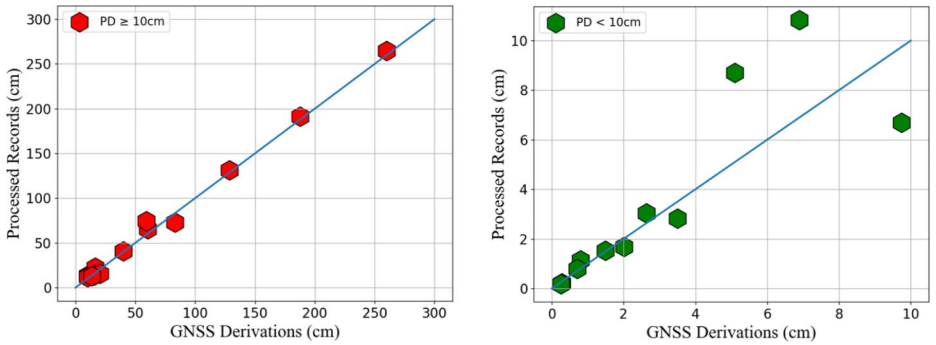


Fig. 4 Comparison of the PDs obtained from strong motion processing with the proposed method and those derived from GNSS data in the literature (left) PD ≥ 10 cm and (right) PD < 10 cm

Table 1 Comparison of PDs obtained on the processed recordings and those derived from GNSS data. PD, PD; SoF, style of faulting. Y01:Yu et al. (2001). K18: Konca et al. (2018), INGV16:INGV (2016), D21: Doğru et al. (2021), P24: Provost et al. (2024)

Date	Earthquake	Mw	SoF	Component	Station	PD (cm)	GNSS Station	PD (cm)	Reference
20.09.1999	Chi-Chi	7.6	TF	EW	TCU137	−264.78	G099	−260	Y01
20.09.1999	Chi-Chi	7.6	TF	EW	TCU074	−191.03	HTZS	−187.7	
20.09.1999	Chi-Chi	7.6	TF	NS	TCU074	131.41	HTZS	128.4	
20.09.1999	Chi-Chi	7.6	TF	UD	TCU074	−65.48	HTZS	−60.3	
20.09.1999	Chi-Chi	7.6	TF	UD	TCU076	−15.63	AF11	−17.7	
20.09.1999	Chi-Chi	7.6	TF	NS	TCU102	−74.56	G103	−59.2	
20.09.1999	Chi-Chi	7.6	TF	UD	TCU102	−13.56	G103	−10	
20.09.1999	Chi-Chi	7.6	TF	NS	TCU078	72.73	M 408	83.2	
20.09.1999	Chi-Chi	7.6	TF	UD	TCU078	−22.7	M408	−16.3	
20.09.1999	Chi-Chi	7.6	TF	UD	TCU120	−14.03	M365	−15.9	
24.05.2014	Aegean Sea	6.9	SS	EW	TK1714	−3.03	CANA	−2.63	K18
24.05.2014	Aegean Sea	6.9	SS	NS	TK1714	1.53	CANA	1.49	
17.11.2015	Lefkada	6.5	SS	EW	KASA	0.22	KASI	0.28	C16
17.11.2015	Lefkada	6.5	SS	NS	LXRA	0.17	KEFA	0.25	
30.10.2016	Norcia	6.6	NF	UD	IVT1214	−40.81	RIFP	−40.15	INGV1
30.10.2016	Norcia	6.6	NF	EW	IVT1214	−11.8	RIFP	−10.02	
30.10.2016	Norcia	6.6	NF	EW	IVT1216	−10.83	MUVI	−6.9	
12.06.2017	Bodrum-Kos	6.6	NF	NS	TK4809	15.79	BOD2	20.51	K19
12.06.2017	Bodrum-Kos	6.6	NF	UD	TK4809	1.14	BOD2	0.8	
12.06.2017	Bodrum-Kos	6.6	NF	NS	TK4812	−2.83	DATC	−3.5	
24.01.2020	Sivrice	6.7	SS	EW	TK2104	1.69	ERGN	2.01	D21
30.10.2020	İzmir(Samos)	7	NF	NS	TK3528	8.7	CESM	5.1	B21
30.10.2020	İzmir(Samos)	7	NF	NS	TK3536	6.7	SFRH	9.74	
30.10.2020	İzmir(Samos)	7	NF	NS	GMLD	12.61	HZUR	13.66	
30.10.2020	İzmir(Samos)	7	NF	EW	KUSD	−0.8	KUSD	−0.7	
02.06.2023	Kahramanmaraş	7.7	SS	RotD100	TK3137	−150.43	P43[a]	150[2]	P24

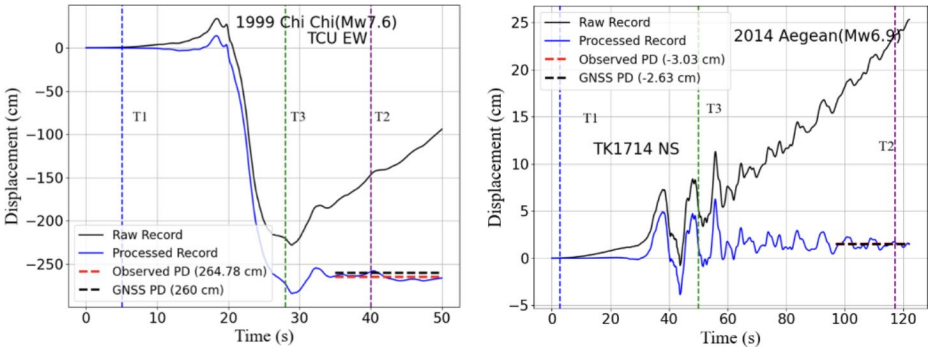


Fig. 5 Comparisons of the PDs on the displacement time histories of (left) the 1999 Chi-Chi earthquake (Mw7.6) station TCU 137- EW component and (right) the 2014 Aegean Sea earthquake (Mw6.9) station TK 1714 -NS component with their assigned time correction points and co-located GNSS stations

slip earthquake, earthquake NS component of station TK 1714 with PD levels derived from co-located GNSS stations.

In addition to GNSS value, PDs are also validated through site observations for the Kahramanmaraş (Mw7.7) earthquake. As an example, the comparison of the PD that emerged in the RotD100 direction at station TK 3137 with the PD derived from satellite data by Provost et al. (2024) is presented in Table 1.

3 Fling inventory of strong motion dataset of Türkİye

In this section, the fling amplitude of the recordings in the strong motion data set of Türkiye has been extracted with the improved eBASCO methodology explained in the methodology section. The selection criteria for the SGM recordings likely to contain a fling step are as follows:

(1) Shallow crustal earthquakes with a depth of at most 30 km;
(2) Earthquakes with a magnitude of 6 and above;

(3) Ground motion recordings within 50 km from the rupture trace ($R_{JB} <= 50$ km).

A total number of 456 (EW, NS, UD) raw recordings meeting the above criteria are obtained from the Earthquake Research Department of the General Directorate of Disaster Affairs (AFAD, https://tadas.afad.gov.tr/list-waveform, last accessed December 2022) and Engin eering Strong Motion Database (ESM, https://esm-db.eu/#/waveform/search, last accessed in December 2022). A summary of the earthquakes utilized in this section is presented in Table 2. Firstly, all recordings within the study limit are visually inspected and recordings containing non-stationary noise such as the NS component of the SKR station from the 1999 Kocaeli earthquake, are eliminated. Then, the remaining 449 recordings are utilized for the rest of the study. The distribution of the earthquakes and stations with the style of faulting as well as the magnitudes are presented in Fig. 6. Although the earthquake dataset mainly consists of strike-slip (SS) earthquakes, the number of normal faulting (NF) earth-

Table 2 Summary of earthquakes and Number of Data Incorporated into the study. Mw: moment magnitude; SoF: style of Faulting; SS: Strike-Slip; N: normal; R: reverse; ISC: International Seismological Center; GCMT: global centroid moment Tensor Project; CSEM: Centre Sismologique Euro-Mediterraneen; AUST: Geoscience Australia. (mw, depth, and SoF information are taken from AFAD.)

Date	Earthquake	Mw	Depth (km)	SoF	Strike/Dip/Rake (°)	Reference of Focal Mechanism	# of Stations/Recordings
10/30/83	Horasan-Narman	6.6	16.1	SS	231/80/21	Pınar (1995)	1/3
03/13/92	Erzincan	6.6	22.6	SS	123/86/175	ISC(GCMT)	1/1
11/06/92	Doğanbey-Izmir	6	17.2	SS	143/83/−21	ISC(GCMT)	2/6
10/01/95	Dinar	6.1	15	NF	136/43/273	Wright et al.(1999)	3/7
06/27/98	Adana-Ceyhan	6.2	25	SS	58/79/11	ISC(CSEM)	1/3
07/31/98	Adana	6.2	32	SS	53/81/15	GCMT	6/18
08/17/99	Izmit (Kocaeli)	7.6	20.7	SS	91/87/164	GCMT	13/37
11/12/99	Düzce	7.1	15.7	SS	268/65/−170	ISC(CSEM)	14/42
06/06/00	Ankara-Çankırı	6	10	SS	2/46/−29	Taymaz and Tan (2001)	1/3
02/03/02	Afyon-Sultandağ	6.5	10	NF	277/60/−51	ISC(CSEM)	1/3
05/01/03	Bingöl	6.3	10	SS	333/67/−171	GCMT	1/3
03/08/10	Elazığ	6.1	5	SS	54/80/−10	Tan et al.(2011)	1/3
10/23/11	Van-Erciş	7.1	15	RV	24/38/60	GCMT	1/3
06/10/12	Fethiye	6.1	24	SS	212/78/3	Dogan et al. (2016)	2/6
05/24/14	Aegen Sea	6.9	12	SS	73/85/−177	GCMT	6/18
06/12/17	Midilli	6.3	7	NF	125/42/−71	Kiratzi (2018)	3/9
07/20/17	Bodrum	6.6	7	NF	275/37/−80	Karasozen et al. (2018)	9/27
01/24/20	Elazığ-Sivrice	6.7	12	SS	244/68/−9	Taymaz et al. (2021)	10/30
10/30/20	Izmir(Samos Island)	7	8.2	NF	270/45/−89	Cetin et al. (2020)	11/33
11/23/22	Düzce(Gölyaka)	6	6.81	SS	255/83/178	ISC(AUST)	11/33
02/06/23	Kahramanmaraş	7.7	8.6	SS	320/80/160	GCMT	36/107
02/06/23	Kahramanmaraş-Ekinözü	7.5	7	SS	358/84/−132	GCMT	6/18
02/20/23	Hatay-Yayladağı	6.3	12	SS	227/45/−16	GCMT	12/36
	# of earthquake	23				# of station/record	152/449

quakes should not be ignored. Fling step studies traditionally focused on reverse (RV) and SS earthquakes due to the scarcity of NF earthquake recordings until the 2016 Norcia/Italy earthquake. D'Amico et al. (2018) identified fling steps in approximately 100 recordings from this event. Although the NF earthquakes have been studied in the subsequent years, the number of available recordings that show PDs remains limited. For instance, D'Amico et al. (2021) studied all the earthquakes that took place between 1950 and 2022 in terms of fling steps and found only 14 NF earthquakes that produced fling within the R_{JB} distance of 140 km.

The PDs of 449 recordings of 152 stations across 23 earthquakes in Turkiye, occurring between 1983 and 2023, are obtained using the scheme explained in the Methodology Section. Calculations are performed for both horizontal and vertical components (EW, NS, UD) as well as fault normal (FN) and fault parallel (FP).

Each processed recording displayed the PD at the end of the record, with detailed earthquake and station information provided in Supplementary Material, Table S1. This supports

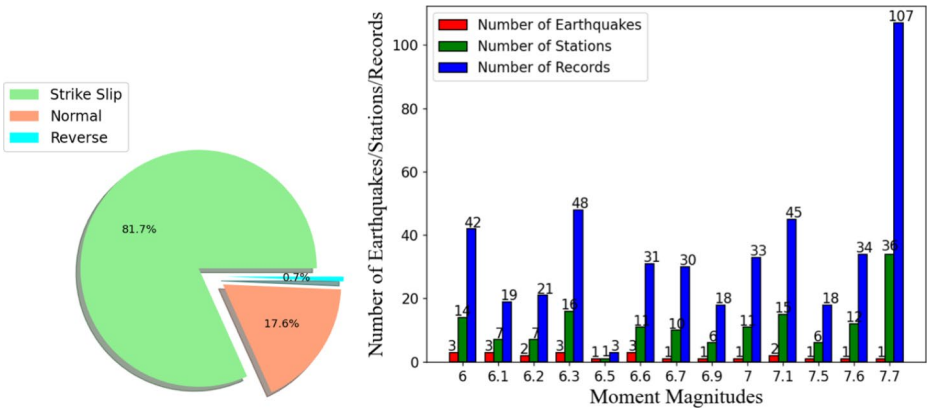


Fig. 6 Distributions of the earthquakes in the dataset with respect to (left) style of faulting and (right) moment magnitudes

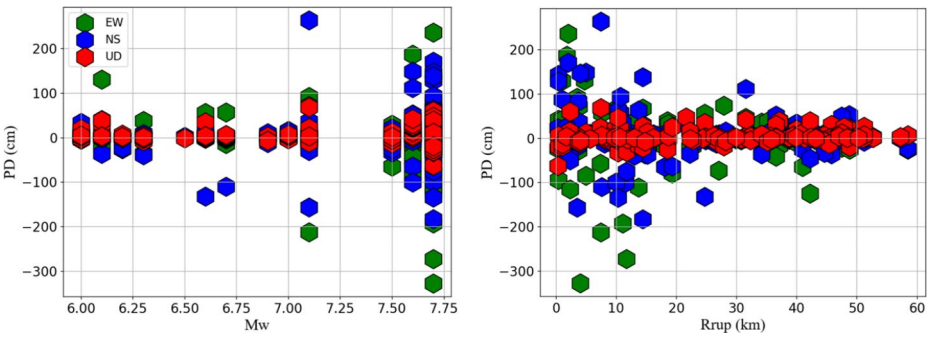


Fig. 7 PDs of main components (EW, NS, UD) with respect to (left) Mw and (right) Rrup

Alavi and Krawinkler (2001)'s statement that all near-fault recordings should contain PD due to the static dislocation area of the earthquake. In addition, PDs in RotD100 directions are calculated at stations with horizontal PD of 10 cm or greater, as presented in Supplementary Material, Table S2. The created dataset promises future studies that can be done by using the proposed study. In Türkiye, only 29 out of 449 records, corresponding to 6.5% of the main component (EW, NS, UD) records, required additional baseline correction as described in Step 4 of the procedure. Those recordings are given in Supplementary Material, Table S3.

Figure 7 illustrates the distribution of PDs of horizontal and vertical components with respect to Mw and R_{RUP}. As expected, the higher the magnitudes result in larger PDs, and closer distances also lead to larger PDs. The largest fling, measuring 327,68 cm, is observed in the EW component of TK 2708 (R_{JB}=3.7 km) during the 2023 Kahramanmaraş (Mw7.7) earthquake.

Interestingly, PDs for the 1999 Düzce earthquake (Mw7.1) in the horizontal components of the station TK 8101 (R_{JB}=3.7 km) are found as 212.66 cm and 263.89 cm. Previous fling studies of this earthquake (Schiappapietra et al. 2021, 2022; D'Amico et al. 2021; Kalkan

et al. 2004) did not include recordings of this station. However, the findings of Yılmaz and Türer (2002), which report PD observation of 2–2.5 m at the location of the Bolu viaduct, support the revealed fling value.

The largest PDs in FN and FP directions are again found during the 2023 Kahramanmaraş earthquake at stations TK 3138 (R_{JB}=2 km) and TK 3145 (R_{JB}=3.7 km) as 307.12 cm and 316.39 cm, respectively. Other PDs are presented in Fig. 8. It is important to note that contrary to the most common definition of the fling step, which states that the fling step is expected to be seen in strike parallel directions (Somerville, 1997, Somerville 2002; Stewart, 2002, Abrahamson 2002; Mena and Mai, 2011, Moghimi and Akkar 2017; Yadav and Gupta 2017), this study has observed fling step in both directions. In some cases, PDs in the FN direction of the SS earthquakes are found larger than those in the FP direction. For example, the 2023 Kahramanmaraş earthquake PDs in the FN and FP directions of TK 4612 are found as 34.65 cm and 13.45 cm, respectively. Similarly, during the 1999 Düzce earthquake, PDs in the FN and FP directions of the station TK 8101 are 215.09 cm and 11.01 cm, respectively.

Kamai et al. (2014), proposed a prediction equation considering RotD100 direction. They ignored the PDs smaller than 10 cm considering the larger uncertainty in the estimation process. In line with this, recordings with horizontal component PDs of 10 cm or are chosen and PDs at RotD100 components are calculated following Somerville (2002) (Fig. 9). 77 RotD100 components are determined among 27,720 processed waveforms. The largest PD is found at TK3138 as 460 cm during the 2023 Kahramanmaraş earthquake.

The presented fling inventory is expected to contribute to the structural design studies, as the only known method of introducing the fling step into seismic design involves selecting and scaling the fling-containing waveform in non-linear time history analyses ((IBC, ICBO 2006), California Building Code (CBC, ICBO 2007), ASCE7-22 (ASCE 2005). Additionally, the PDs presented could give implications for geotechnical aspects of the earthquakes. For instance, Çetin et al. (2023) observed liquefaction formations during the 2023 Kahramanmaraş earthquake at the locations of the TK3132 and TK4625, which may be responsible for the large PDs (173 cm and 245 cm) in RotD100 direction, respectively. Furthermore, Rathje et al. (2006) indicated that the 1999 Düzce earthquake caused a landslide at station C375, which was located on a steep hillside, where the PD in the RotD100 direction is found to be 197 cm.

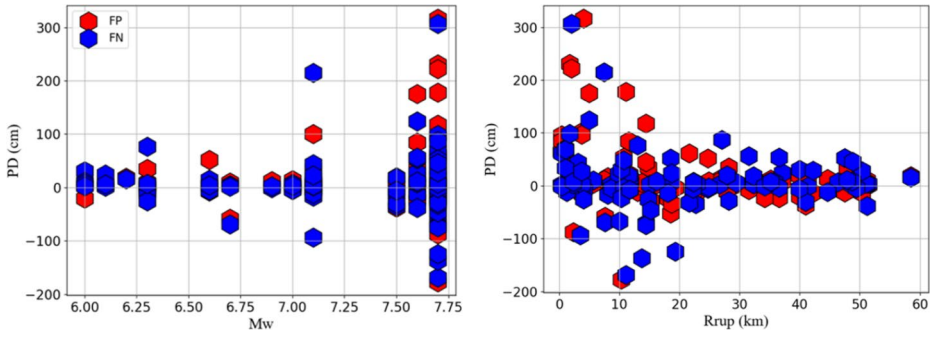


Fig. 8 Distribution of the PDs in the FP and FN directions with respect to (left) Mw and (right) Rrup

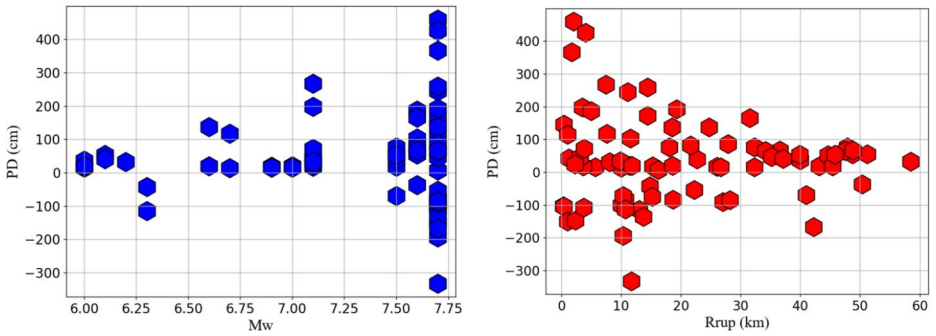


Fig. 9 Distribution of the PDs in the RotD100 directions with respect to (left) Mw and (right) Rrup

4 Comparison with fling step amplitude prediction models

In this section, the estimation capacities of three fling prediction models—Kamai et al. (2014), Burks and Baker (2016), and Schiappapietra et al. (2022)—are evaluated for Türkiye. All three models are inspired by the work of Byerly and DeNoyer (1958), who modelled surface displacement as a function of distance for the 1906 San Francisco earthquake, and Abrahamson (2002), who mathematically described the fling step for strike-slip earthquakes. Additionally, all three models are based on earthquake simulations. Moreover, while Kamai et al. (2014) and Schiappapietra et al. (2022) consider fault style as a predictive parameter, Burks and Baker (2016) do not include this factor in their model. This difference stems from the fact that Kamai et al. (2014) developed their predictive model using different simulation sets, and although they acknowledged the influence of fault style on the fling step pulse period, they did not address its effect on the permanent displacement (PD).

For the evaluation of the performances of these models, the PDs in Türkiye fling step inventory, presented in the previous section, are estimated by each one of the prediction models. The residual values of PDs in slip directions are calculated using three prediction equations and the fling inventory by following Gülerce et al. (2016) by considering each record (i) from each event (j) as follows:

$$R_{ij} = ln\left(a_{ij}\right) - ln\left(p_{ij}\right) = c_k + {}_{Bj} + {}_{Wij} \tag{7}$$

where R_{ij} is the total residual, a_{ij} is the permanent displacement observed on the processed record and p_{ij} is the predicted value. The total residual is divided into three parts: c_k, the average bias of the real permanent displacements relative to predicted ones, Δ_{Bj}, inter-event residuals, and Δ_{Wj}, intra-event residuals.

5 Burks and Baker (2016)

Burks and Baker (2016) presented a single fling step prediction model for all styles of faulting earthquakes by using only two input parameters as follows:

$$ln\left(D_P\right) = ln\left(\cot^{-1}\left(0.3R\right)\right) + 1.3Mw - 5.1 \tag{8}$$

where R is the R_{RUP} distances of the stations in km, Mw is the moment magnitudes of the earthquakes, and D_P is the estimated fling amplitude in cm. This model was designed to estimate PDs in the fault parallel (FP) direction of SS and fault normal (FN) direction of dipping earthquakes. Therefore, the slip direction components in the compiled dataset are utilized to evaluate the performance of this model. In this process, PDs larger than 3 cm are considered, from a given engineering perspective. As a result, 92 (81 SS + 11 N) from 18 earthquakes are utilized in this stage of the study. The intra-event and inter-event residual plots are presented in Fig. 10. It is clear from the figure that this model underestimates smaller earthquakes whereas it better estimates larger ones.

6 Kamai et al. (2014)

Kamai et al. (2014) prediction model was constructed for the RotD100 direction of the SS and RV earthquakes. Due to the scarcity of RV earthquakes in the Türkiye SGM database in the given range, only the fling step prediction model for SS earthquakes, given in Eq. 9, is evaluated.

$$log\left(\frac{D_{site}}{D_{fault}}\right) = log\left(0.005\delta + 0.05 + a\left(1.35 - 0.015\delta\right)\right) + \left(25.29Mw - 1.577Mw^2 - 106.22 + 0.02\delta\right) log\left(\frac{R_{RUP}+50}{50}\right) \quad (9)$$

$$D_{fault} = \frac{M_0}{\mu\, LW} \quad (10)$$

where M_0 is the seismic moment in a unit of dyn.cm, L, and W are the rupture length and width in cm, respectively. Rupture area (L x W) of each earthquake is either obtained directly from previous studies or calculated based on Wells and Coppersmith (1994). In addition, μ is the rigidity of the fault surface in dyn/cm^2, which is assumed as 3×10^{11} dyn/cm^2. Event specific parameters, magnitudes, dip angles, seismic moments and rupture areas (L x W) are presented with site specific Rx distances in Supplementary Material, Table 2.

The performance of this prediction model is evaluated with 72 recordings from 11 SS earthquakes by conducting residual analyses. The resulting inter-event and intra-event residuals of PD are demonstrated in Fig. 11. A general underestimation of PD is apparent at

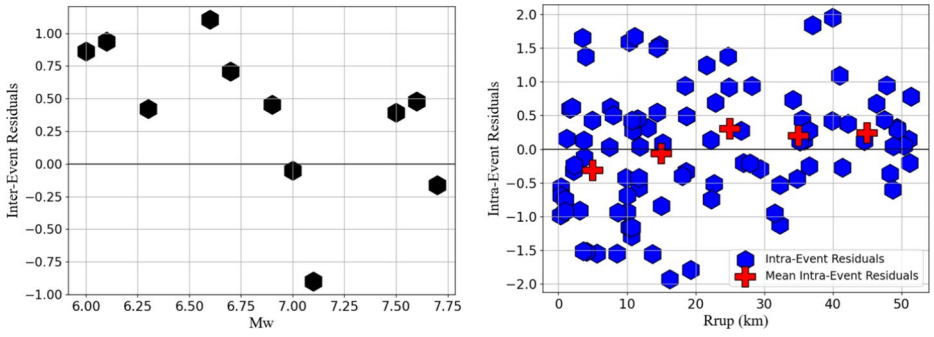


Fig. 10 (Left) Inter-event and (right) intra-event residuals of PD predicted with Burks and Baker (2016)

all magnitude ranges. The model gives rise to better estimates for large earthquakes In terms of intra-event residuals overestimation is observed for close location to the fault rupture trace. This prediction model is found open for improvement even though the calculation of RotD100 directions makes it difficult. Satoh (2020) inspected the approximations of Kamai et al. (2014) for 6 Japan earthquakes and presented a new seismic moment-rupture area relation using the homogeneous-slip models from geodetic data to be substituted in the model instead of Wells and Coppersmith (1994). However, for some Türkiye earthquakes, this approximation does not result in better estimates. For instance, the PD predictions of Kamai et al. (2014) and Satoh (2020) for the 1999 Kocaeli earthquake YPT station, whose PD in RotD100 is presented as 187.43 in this study, are found as 188.41 cm and 119.53 cm, respectively.

6.1 Schiappapietra et al. (2022)

Schiappapietra et al. (2022) developed a fling amplitude prediction model for the RotD100 direction as:

$$\begin{aligned} log_{10}PDS = &-4.57 + 0.07HW + 1.89Mw - 0.1Mw^2 - 1.16log_{10}\left(R_{RUP} + h\right) \\ &- 0.32log_{10}\left(\delta\right) - 0.09NF + 0.03TF \end{aligned} \tag{11}$$

Although input parameters are similar to those in Kamai et al. (2014), this prediction model is also valid for NF earthquakes. Consequently, the performance of the model is evaluated with all the RotD100 recordings presented in Fig. 9 (77 recordings from 14 earthquakes) by conducting residual analyses. Figure 12 shows the inter-event and intra-event residuals of PD. It is found that Schiappapietra et al. (2022) better estimates the PDs in close distances than Kamai et al. (2014). To exemplify, while the mean intra-event residual within the first 10 km is 0.23 for Kamai et al. (2014), it is found as 0.18 for Schiappapietra et al. (2022). In addition, apart from, the 2023 Türkiye earthquake sequence, the PD predictions for large earthquakes are found successful.

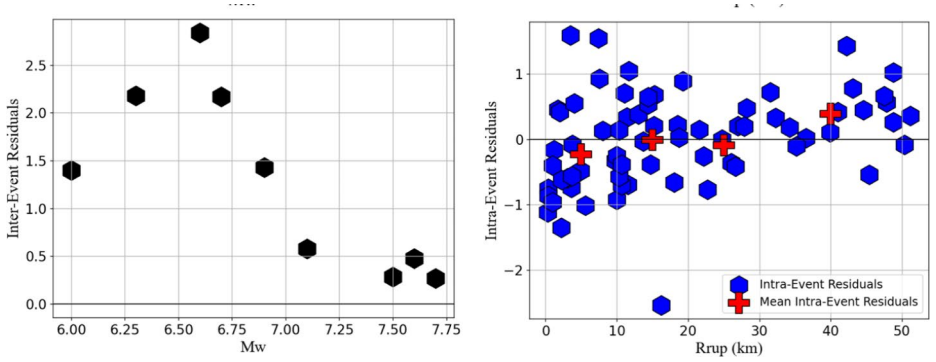


Fig. 11 (Left) Inter-event and (right) intra-event residuals of PD predicted with Kamai et al. (2014)

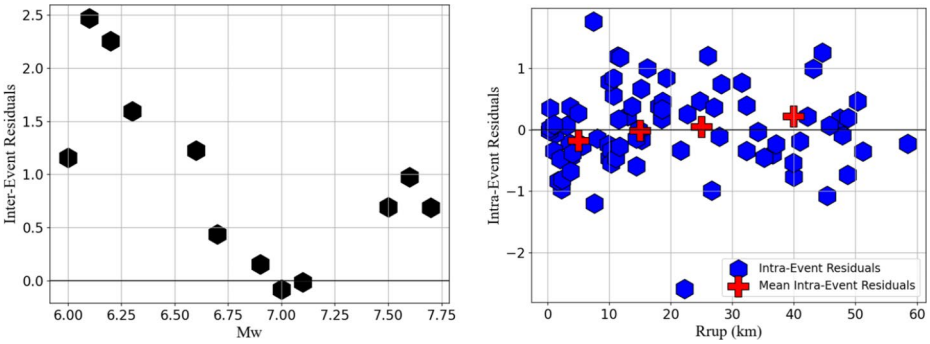


Fig. 12 (Left) Inter-event and (right) intra-event residuals of PD predicted with Schiappapietra et al. (2022)

7 Turkiye adjusted version of Burks and Baker (2016) prediction model

The performance of the Burks and Baker (2016) fling step predictive model, particularly for moderate and small earthquakes, is found to be relatively better than both the Kamai et al. (2014) and Schiappapietra et al. (2022) models. The feasibility and the predictive ability of Burks and Baker (2016) are promising; however, improvements are necessary to minimize discrepancies and enhance its applicability in earthquake engineering. Therefore, Burks and Baker (2014) fling step prediction equation is refined for Türkiye through random-effects regression analyses, utilizing residual plots for adjustments.

The refinement process involves removing the observed trends from the residual graphics. Initially, a trend in the inter-event residual plot is observed, leading to the fitting of an adjustment function to the total event terms, thereby modifying the original prediction model. The updated model is then subjected to repeated residual analysis. Upon identifying another trend in the intra-event residual plot, the adjustment procedure continues with another fitting function, further refining the prediction equation. This modification sequence, defined as a cycle, is repeated until the trends are no longer visible in the residual plots. Additionally, since the scatter of intra-event residuals is found considerably different in the first 10 km than in others, the prediction equation is evaluated in two segments: 0–10 km and 10–50 km. The final adjustment procedure comprises six cycles, resulting in the following proposed fling amplitude prediction equation:

$$ln\left(D_P\right) = ln\left(\cot^{-1}\left(0.3R\right)\right) + 0.6953Mw + 0.01394R - 0.8249 - N(0.05334R + 0.1114) \quad (12)$$

where R is the R_{RUP} distances of the stations in km, Mw is the moment magnitudes of the earthquakes, N is the dummy variable for and equal to 1 for R_{RUP} of 0–10 km and equal to 0 for R_{RUP} of 10–50 km, and D_P is the estimated fling amplitude in cm. This refined prediction equation provides better estimates for the Türkiye fling inventory compared to existing models. To exemplify, while the inter-event residuals from the original model ranged between −1 and 1, those from the adjusted model were found from −0.6 to 0.6. Similarly, the mean values of the intra-event residuals are found between 0.13 and −0.06, aligned closely with the zero line in the graphs.

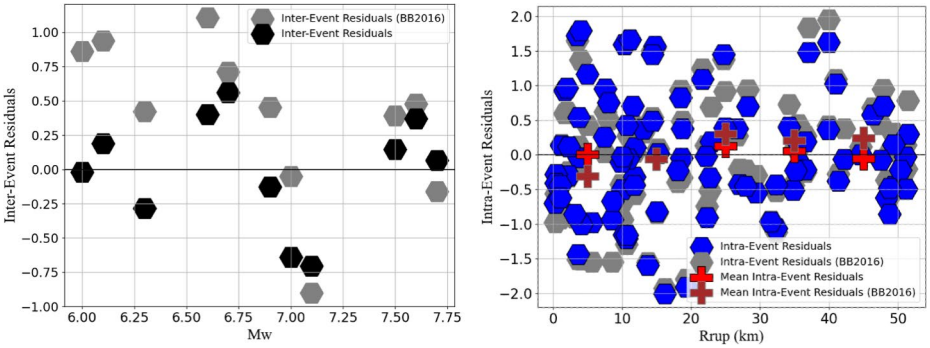


Fig. 13 (Left) Inter-event and (right) intra-event residuals of PD for Türkiye predicted with adjusted Burks and Baker (2016) and with the original Burks and Baker (2016) model

It is important to note that because the Burks and Baker (2016) model is valid for the slip direction components of the earthquakes, the modifications are made considering the FP component of SS events and the FN component of normal faulting events. Residual plots of the proposed prediction model are presented in Fig. 13.

8 Conclusion

In this study, an enhanced data processing scheme for recovering the fling step is introduced, addressing limitations observed in the previous procedures while significantly reducing computational load. Validation of the scheme against co-located GNSS data from Turkish and worldwide earthquakes demonstrates its robust capability across a wide range of permanent displacements. Although the procedure is found to be highly successful, the flatness of the initial part of the recording could also be considered in the selection of the best result, rather than relying solely on fade level, based on the general step function shape definition.

Processing near fault recordings from Türkiye earthquakes has led to the development of a comprehensive Türkiye fling inventory. Integrating these findings into NESS 2.0 (D'Amico et al. 2021), the global repository for fling containing seismic recordings could potentially increase its coverage by 62% and 22% for SS and NF earthquakes, respectively.

The presented inventory is also used to evaluate existing fling-step prediction equation models in Türkiye, revealing their limitations due to insufficient observed data during model construction. Consequently, a novel fling step prediction model has been proposed by adapting Burks and Baker's framework to Türkiye's specific fling inventory.

While this study primarily focuses on Türkiye earthquakes, future research should aim to expand the fling database globally. Establishing a more comprehensive dataset that includes worldwide earthquakes would enhance the predictive accuracy and applicability of fling-step models across diverse seismic regions. In addition, although no need is encountered in this study, the selection of the best result can be improved by accounting for the flatness level of the initial part of a recording, rather than solely on the fade level, based on the general step function shape definition.

Supplementary Information The online version contains supplementary material available at https://doi.org/10.1007/s10518-024-02094-6.

Funding Open access funding provided by the Scientific and Technological Research Council of Türkiye (TÜBİTAK).

Declarations

Conflict of interest The authors declare that they have no known competing financial interests or personal relationships that could have appeared to influence the work reported in this paper.

Open Access This article is licensed under a Creative Commons Attribution 4.0 International License, which permits use, sharing, adaptation, distribution and reproduction in any medium or format, as long as you give appropriate credit to the original author(s) and the source, provide a link to the Creative Commons licence, and indicate if changes were made. The images or other third party material in this article are included in the article's Creative Commons licence, unless indicated otherwise in a credit line to the material. If material is not included in the article's Creative Commons licence and your intended use is not permitted by statutory regulation or exceeds the permitted use, you will need to obtain permission directly from the copyright holder. To view a copy of this licence, visit http://creativecommons.org/licenses/by/4.0/.

References

Abrahamson NA (2002) Velocity Pulses in Near-Fault Ground Motions. Proceedings of the UC Berkeley—CUREE Symposium in Honor of Ray Clough and Joseph Penzien: Berkeley, California, UC Berkeley, Consortium of Universities for Research in Earthquake Engineering, pp. 40–41

Alavi B, Krawinkler H (2001) Effects of near-fault ground motions on frame structures. Report No. 138. California. The John A. Blume Earthquake Engineering Center, Stanford University

American Society of Civil Engineers (2005) ASCE-7 Minimum Design Loads for Buildings, Reston, VA

Beyer K (2006) Relationships between median values and between aleatory variabilities for different definitions of the horizontal component of motion. Bull Seismol Soc Am 96(4A):1512–1522. https://doi.org/10.1785/0120050210

Bhagat S, Wijeyewickrema AC, Subedi N (2021) Influence of Near-Fault Ground motions with Fling-Step and Forward-Directivity characteristics on seismic response of base-isolated buildings. J Earthquake Eng 25(3):455–474. https://doi.org/10.1080/13632469.2018.1520759

Birgören G, Sekiguchi H, Irikura K (2004) Rupture model of the 1999 Düzce, Turkey, earthquake deduced from high and low frequency strong motion data. Geophys Res Lett 31(5). https://doi.org/10.1029/2003gl019194

Boore DM (1999) Effect of baseline corrections on response spectra for two recordings of the 1999 Chi-Chi, Taiwan, earthquake. Open-File Report / 1999. https://doi.org/10.3133/ofr99545

Boore DM (2001) Effect of baseline corrections on displacements and response spectra for several recordings of the 1999 Chi-Chi, Taiwan. Earthq Bull Seismological Soc Am 91(5):1199–1211

Boore DM, Bommer JJ (2005) Processing of strong-motion accelerograms: needs, options and consequences. Soil Dynamics and Earthquake Engineering 2005; 25(2): 93–115. https://doi.org/10.1016/j.soildyn.2004.10.007

Building Seismic Safety Council (BSSC) (1998) 1997 Edition NEHRP Recommended Provisions for Seismic Regulations for New Buildings and Other Structures, FEMA 303, prepared for the Federal Emergency Management Agency, Washington, DC

Burks LS, Baker JW (2014) Fling in near-fault ground motions and its effect on structural collapse capacity. Proceedings of the 10th National Conference in Earthquake Engineering, Earthquake Engineering Research Institute, Anchorage, AK

Burks LS, Baker JW (2016) A predictive model for fling-step in Near-fault ground motions based on recordings and simulations. Soil Dyn Earthq Eng 80:119–126

Byerly P, DeNoyer J (1958) Energy in earthquakes as computed from geodetic observations. Contributions in Geophysics in Honor of Beno Gutenberg, vol 1. Pergamon, New York, pp 17–35

Cetin KO, Mylonakis G, Sextos A, Stewart JP (2020) Seismological and engineering effects of the M 7.0 Samos Island (Aegean Sea) Earthquake, GEER Report 069, Hellenic Association of Earthquake Engineering. Earthquake Engineering Association of Turkey. Earthquake Foundation of Turkey, Earthquake Engineering Research Institute, Geotechnical Extreme Event Reconnaissance Association

Cetin KO, Ilgac M, Can G, Cakir E (2023) Preliminary Reconnaince Report on February 6, 2023, Pazarcik Mw7.7 and Elbistan Mw7.6 KahramanmarasTurkiye earthquakes. METU/EERC 2023- 01, Middle East. Technical University and Earthquake Engineering Research Center, Türkiye

Chao W, Wu Y, Zhao L (2010) An automatic scheme for baseline correction of strong-motion records in coseismic deformation determination. Journal of Seismology 2010; 14(3): 495–504. https://doi.org/10.1007/s10950-009-9178-7

D'Amico MC, Schiappapietra E, Felicetta C, Sgobba S, Pacor F, Lanzano G, Russo E, Luzi L (2021) NEar-Source strong-motion flatfile from eBASCO (NESS-eBASCO), version 2.0 (Version 2.0) [Data set]. Istituto Nazionale di Geofisica e Vulcanologia (INGV)

D'Amico M, Felicetta C, Schiappapietra E, Pacor F, Gallovič F, Paolucci R, Puglia R, Lanzano G, Sgobba S, Luzi L (2018) Fling effects from Near-Source strong-motion recordings: insights from the 2016 mw 6.5 Norcia, Central Italy, Earthquake. Seismol Res Lett 90(2A):659–671. https://doi.org/10.1785/0220180169

Dhanya J, Raghukanth ST (2020) Probabilistic fling hazard map of India and adjoined regions. J Earthquake Eng 26(9):4712–4736. https://doi.org/10.1080/13632469.2020.1838969

Disaster and Emergency Management Authority (1973) Turkish national strong Motion Network. Data set. https://doi.org/10.7914/SN/TK. Department of Earthquake, Disaster and Emergency Management Authority

Doğan B, Irmak TS, Karakaş A, Kalafat D (2016) Seismo-tectonic content by the source parameters of the 10 June 2012 Ölüdeniz-Fethiye (Dodecanese Islands) Mw 6.1 earthquake and aftershocks (SW-Turkey). Acta Geod Geoph 51:15–41

Doğru A, Bulut F, Yaltırak C, Aktuğ B (2021) Slip distribution of the 2020 Elazığ Earthquake (Mw 6.75) and its influence on earthquake hazard in the Eastern Anatolia. Geophys J Int 224(1):389–400. https://doi.org/10.1093/gji/ggaa471

Dziewonski AM, Chou TA, Woodhouse JH (1981) Determination of earthquake source parameters from waveform data for studies of global and regional seismicity. J Geophys Res 86:2825–2852. https://doi.org/10.1029/JB086iB04p02825

Erdik M (1999) Report on 1999 Kocaeli and Düzce (Turkey) earthquakes. Istanbul Boğaziçi University

Erdik M (2001) Report on 1999 Kocaeli and Duzce (Turkey) earthquakes. In: Casciati F, Magonette G (eds) Structural control for civil and infrastructure engineering. World Scientific, Singapore

Geospatial Information Authority of Japan (2023) The 2023 Turkey Earthquake: Crustal deformation detected by ALOS-2 data. https://www.gsi.go.jp/cais/topic20230206e_Turkey.html, Accessed on March 3, 2023

Gholipour A, Davoodi M, Yousefpour H (2023) Effects of Fling Step on the seismic response of Reinforced concrete Arch bridges. Struct Build (Proceedings ICE). https://doi.org/10.1680/jstbu.23.00040

Gülerce Z, Kargıoğlu B, Abrahamson NA (2016) Turkey-adjusted NGA-W1 Horizontal Ground Motion Prediction models. Earthq Spectra 32:75–100

Hamidi H, Khosravi H, Soleimani R (2018) Fling-step ground motions Simulation using theoretical-based Green's function technique for structural analysis. 115:232–245Soil Dynamics and Earthquake Engineering

Hisada Y, Bielak JA (2003) Theoretical method for Computing Near-Fault Ground motions in layered half-spaces considering Static Offset due to Surface Faulting, with a physical interpretation of Fling Step and Rupture Directivity. Bull Seismol Soc Am 93(3):1154–1168. https://doi.org/10.1785/0120020165

Hisada Y, Tanaka S (2021) What Is Fling Step? Its Theory, Simulation Method, and Applications to Strong Ground Motion near Surface Fault Ruptures. Bulletin of the Seismological Society of America 2021; 111(5): 2486–2506. https://doi.org/10.1785/0120210046

INGV16: Istituto Nazionale di Geofisica e Vulcanologia (INGV) Working Group (2016) GPS Geodesy (GPS Data and Data Analysis Center). Preliminary co-seismic displacements for the October 26 (mw 5.9) and October 30 (mw 6.5) Central Italy Earthquakes from the Analysis of GPS Stations

International Conference of Building Officials ICBO (2006) 1973 Uniform Building Code, Whittier, CA

International Conference of Building Officials ICBO (2007) 1973. Uniform Building Code, Whittier, CA

Iwan WD, Möser M, Peng CY (1985) Some observations on strong-motion earthquake measurement using a digital accelerograph. Bull Seismol Soc Am 75(5):1225–1246. https://doi.org/10.1785/bssa0750051225

Jamnani HH, Karbassi A, Lestuzzi P (2013) Fling-step effect on the seismic behaviour ofhigh-rise RC buildings during the Christchurch earthquake. 2013 NZSEE Conference

Jin S, Wang D, Jiang D (2023) Seismic fragility analysis of containment structure subjected to near fault ground motions. Prog Nucl Energy 161:104734. https://doi.org/10.1016/j.pnucene.2023.104734

Kaklamanos J, Baise LG, Boore DM (2011) Estimating unknown input parameters when implementing the NGA Ground Motion prediction equations in Engineering Practice. Earthq Spectra 27:1219–1235

Kalkan E, Kunnath SK (2006) Effects of Fling step and forward directivity on seismic response of buildings. Earthq Spectra 22(2):367–390. https://doi.org/10.1193/1.2192560

Kalkan E, Adalier K, Pamuk A (2004) Near Field Effects and Engineering Implications of Recent Earthquakes in Turkey. Proceedings of the 5th International Conference on Case histories in Geotechnical Engineering: New York, NY, April 13–17

Kamai R, Abrahamson NA, Graves R (2014) Adding fling effects to processed ground-motion time histories. Bull Seismol Soc Am 104(4):1914–1929. https://doi.org/10.1785/0120130272

Karasözen E, Nissen E, Büyükakpınar P, Cambaz MD, Kahraman M, Ertan EK, Abgarmi B, Bergman E, Ghods E, Özacar AA (2018) The 2017 July 20 mw 6.6 Bodrum–Kos Earthquake illuminates active faulting in the Gulf of Gökova, SW Turkey. Geophys J Int 214:185–199

Kiratzi A (2017) The 12 June 2017 Mw 6.3 Lesvos Island (Aegean Sea) Earthquake: Slip Model and Directivity estimated with Finite-Fault Inversion, vol 725. Tectonophysics, p 724

Konca AO, Cetin S, Karabulut H, Reilinger R, Dogan U, Ergintav S, Cakir Z, Tari E (2018) The 2014 Mw 6.9 North Aegean Earthquake: Seismic and Geodetic evidence for Coseismic Slip on Persistent Asperities. Geophys J Int 213(2):1113–1120

Lentas K, Di Giacomo D, Harris J, Storchak DA (2019) The ISC Bulletin as a comprehensive source of earthquake source mechanisms. Earth Syst Sci Data 11:565–578. https://doi.org/10.5194/essd-11-565-2019

Luzi L, Lanzano G, Felicetta C, D'Amico MC, Russo E, Sgobba S, Pacor F, ORFEUS Working Group 5 (2020) Engineering Strong Motion Database (ESM) (Version 2.0). Istituto Nazionale di Geofisica e Vulcanologia (INGV). https://doi.org/10.13127/ESM.2

Mena B, Martin PM (2011) Selection and quantification of near-fault velocity pulses owing to source directivity. Georisk: Assessment and Management of Risk for Engineered systems and Geohazards. 5(1):25–43. https://doi.org/10.1080/17499511003679949

Moghimi S, Akkar S (2017) Examining the spatial distributions of spectral amplitudes exposed to close fault orientation effects using probabilistic earthquake scenarios. 4th International Conference on Earthquake Engineering and Seismology. October 11–13, Anadolu University, Eskişehir. (in Turkish)

Mortezaei A, Ronagh HR, Kheyroddin A (2010) Seismic evaluation of FRP strengthened RC buildings subjected to near-fault ground motions having fling step. Compos Struct 92(5):1200–1211. https://doi.org/10.1016/j.compstruct.2009.10.017

Pınar A Rupture Process and Spectra of Some Major Turkish Earthquakes and Their Seismotectonic Implications. (, Thesis PD (1995) Boğaziçi University, Istanbul

Provost F, Karabacak V, Malet JP, Meghraoui M, Masson F, Ferry M, Michéa D, Pointal E (2024) High-resolution co-seismic fault offsets of the 2023 Türkiye earthquake ruptures using satellite imagery. Sci Rep 14:6834. https://doi.org/10.1038/s41598-024-55009-5

Rathje EM, Stewart JP, Baturay MB, Bray JD, Bardet JP (2006) Strong ground motions and damage patterns from the 1999 Düzce Earthquake in Turkey. J Earthq Eng 10:693–724

Sasani M, Bertero VV (2000) Importance of severe pulse-type ground motions in performance-based engineering: historical and critical review, World Conference of Earthquake Engineering

Satoh T (2020) Static displacement and long-period velocity pulse of crustal earthquakes in Japan. J Japan Association Earthq Eng 20(5):36–58

Schiappapietra E, Felicetta C, D'Amico M (2021) Fling-step recovering from near-source waveforms database. Geosciences 2021;11:1–22. https://doi.org/10.3390/geosciences11020067

Schiappapietra E, Lanzano G, Sgobba S (2022) Empirical predictive models for fling step and displacement response spectra based on the NESS database. Soil Dyn Earthq Eng. https://doi.org/10.1016/j.soildyn.2022.107294

Shortt ER (1985) (MSc thesis). Source characterization of the October 30, 1983 Narman-Horasan earthquake. Massachusetts Institute of Technology, Massachusetts

Somerville PG (2002) Characterizing near fault ground motion for the design and evaluation of bridges. Third National Seismic Conference & Workshop on Bridges & Highways, Portland, Oregon

Somerville PG, Smith NF, Graves RW, Abrahamson NA (1997) Modification of empirical strong ground motion attenuation relations to include the amplitude and duration effects of rupture directivity. Seismological Res Letter 68(1):199–222

Stewart JP, Chiou SJ, Bray JD, Graves RW, Somerville PG, Abrahamson NA (2002) Ground motion evaluation procedures for performance-based design. Soil Dyn Earthq Eng 22(9–12):765–772

Tan O, Pabuçcu Z, Tapırdamaz MC, İnan S, Ergintav S, Eyidogan H, Aksoy E, Kuluöztürk F (2011) Aftershock study and seismotectonic implications of the 8 March 2010 Kovancılar (Elazığ, Turkey) earthquake (MW = 6.1). Geophys Res Lett 38:L11304

Tanırcan G, Gulerce Z, Tetik T, Akbaş B (2022) Adapting a global fourier amplitude spectrum estimation model to the earthquake database of Turkiye. In TUBİTAK 1002 Project Report No: 120M799, [in Turkish]. (Accessible after 05/2025)

Taymaz T, Tan O (2001) Source Parameters of June 6, 2000 Orta-Çankırı and December 15, 2000 Sultandağı-Akşehir Earthquakes (Mw = 6.0) Obtained from Inversion of Teleseismic Body Wave Forms. Symposia on Seismotectonics of the North–Western Anatolia—Aegean and Recent Turkish Earthquakes: Scientific Activities, pp. 96–107

Taymaz T, Ganas A, Yolsal-Çevikbilen S, Vera F, Eken T, Erman C, Keleş D, Kapetanidis V, Valkaniotis S, Karasante I, Tsironi V, Gaebler P, Melgar D, Öcalan T (2021) Source mechanism and rupture process of the 24 January 2020 Mw 6.7 Doğanyol Sivrice Earthquake Obtained from Seismological Waveform Analysis and Space Geodetic Observations on the East Anatolian Fault Zone (Turkey). Tectonophysics 804:228745

Trifunac MD, Crady AG, A Study on The Duration of Strong Earthquake Ground Motion (1975). Bulletin of the Seismological Society of America 1975; 65(3): 581–626. https://doi.org/10.1785/bssa0650030581

Ucak A, Mavroeidis GP, Tsopelas P (2014) Behavior of a seismically isolated bridge crossing a fault rupture zone. Soil Dyn Earthq Eng 57:164–178. https://doi.org/10.1016/j.soildyn.2013.10.012

Wells DL, Coppersmith KJ (1994) New empirical relationships among Magnitude, rupture length, rupture width, rupture area, and Surface Displacement. Bull Seismol Soc Am 84(4):974–1002. https://doi.org/10.1785/bssa0840040974

Wright TJ, Parsons BE, Jackson JA, Haynes M, Fielding EJ, England PC, Clarke PJ (1999) Source parameters of the 1 October Dinar (Turkey) Earthquake from SAR Interferometry and Seismic Body Wave Modelling. Earth Planet Sci Lett 171:23–37

Wu Y, Wu CF (2007) Approximate recovery of coseismic deformation from Taiwan strong-motion records. J Seismolog 11(2):159–170. https://doi.org/10.1007/s10950-006-9043-x

Wu S, Nozu A, Nagasaka Y (2020) Accuracy of Near-Fault Fling-Step displacements estimated using the discrete Wavenumber method. Bull Seismol Soc Am 111(1):309–320. https://doi.org/10.1785/0120190257

Xue Y, Pu W, Matsuda K, Kasai K (2020) Influence of high-pass filtering of near-fault earthquake record on the responses of base-isolated building. Soil Dyn Earthq Eng 135:106182. https://doi.org/10.1016/j.soildyn.2020.106182

Yadav KK, Gupta VK (2017) Near-fault fling-step ground motions: characteristics and simulation. Soil Dyn Earthq Eng 101:90–104. https://doi.org/10.1016/j.soildyn.2017.06.022

Yang D, Pan J, Li G (2010) Interstory drift ratio of building structures subjected to near-fault ground motions based on generalized drift spectral analysis. Soil Dyn Earthq Eng 30(11):1182–1197. https://doi.org/10.1016/j.soildyn.2010.04.026

Yılmaz C, Türer A (2002) Design philosophy and earthquake behavior of the 2300-meter-long Bolu viaduct 2002; ECAS2002 International Symposium on Structural and Earthquake Engineering: 50–65 (in Turkish)

Yu SB, Kuo LC, Hsu Y, Su HH, Liu CC, Hou CS, Lee JF, Lai TC, Liu CC, Liu CL, Tseng TF, Tsai CS, Shin TC (2001) Preseismic Deformation and Coseismic Displacements Associated with the 1999 Chi-Chi, Taiwan, Earthquake. Bull Seismol Soc Am 91(5):995–1012. https://doi.org/10.1785/0120000722

Publisher's note Springer Nature remains neutral with regard to jurisdictional claims in published maps and institutional affiliations.